

# Effect of high electric fields on the nematic to isotropic transition in a material exhibiting large negative dielectric anisotropy

S. Dhara<sup>1,a</sup> and N.V. Madhusudana<sup>2,b</sup>

<sup>1</sup> School of Physics, University of Hyderabad, Hyderabad 500046, India

<sup>2</sup> Raman Research Institute, C.V. Raman Avenue, Bangalore 560080, India

Received 30 November 2006 / Received in final form 14 February 2007

Published online: 14 March 2007 – © EDP Sciences, Società Italiana di Fisica, Springer-Verlag 2007

**Abstract.** We report the experimental high electric field phase diagram of a nematic liquid crystal which exhibits a large *negative* dielectric anisotropy. We measure simultaneously the birefringence ( $\Delta n$ ) and the dielectric constant ( $\epsilon_{\perp}$ ) at various applied fields as functions of the *local temperature* of an aligned sample. We also measure the higher harmonics of the electrical response of the medium. The following experimental results are noted: (i) enhancement of orientational order parameter  $S$  in the nematic phase due to both the Kerr effect and quenching of director fluctuations; (ii) enhancement in the paranematic to nematic transition temperature ( $T_{PN}$ ) with field; (iii) divergence of the order parameter susceptibility beyond the tricritical point as measured by third harmonic *electrical* signal; (iv) a small second harmonic electrical signal which also diverges near  $T_{PN}$ , indicating the presence of polarised domains. Our measurements show that  $\Delta T_{PN}(= T_{PN}(E) - T_{NI}(0))$  varies *linearly* with  $|E|$  whereas the Landau de Gennes theory predicts a dependence on  $E^2$ . It is argued that the quenching of director fluctuations by the field makes the dominant contribution to all the observations, including the thermodynamics of the transition.

**PACS.** 64.70.Md Transitions in liquid crystals – 61.30.Gd Orientational order of liquid crystals; electric and magnetic field effects on order – 61.30.Dk Continuum models and theories of liquid crystal structure

## 1 Introduction

Liquid crystals are anisotropic fluids, made of molecules which lack spherical symmetry. They exhibit a variety of phase transitions. These transitions can be thermodynamically first or second order in nature [1]. The simplest liquid crystal phase known so far is the uniaxial nematic. When the nematic is made of rod like molecules their long axes exhibit long-range orientational order along a specific direction called the director denoted by  $\hat{n}$ , a dimensionless unit vector.  $\hat{n}$  and  $-\hat{n}$  are indistinguishable and the system does not show any macroscopic polarisation. In the uniaxial nematic phase, the magnitude of the orientational order parameter  $S = \langle 3 \cos^2 \theta - 1 \rangle / 2$  [1], where  $\theta$  is the angle between the long axis of a molecule and the director and angular brackets represent a statistical average. Thermodynamically the isotropic to nematic phase transition is weakly first order with a heat of transition of  $\sim 1$  kJ/mol [1]. Studies on the effects of electric and magnetic fields on liquid crystals are interesting because of both fundamental and technological importance. The weak curvature elasticity of the nematic produces large electrooptic effects exploited by the display industry and also very strong fluctuations of the director which result

in a turbid appearance of a bulk sample [1]. There have been several reports on the effect of strong electric and magnetic fields on the isotropic to nematic phase transition [2–9]. The electric field experiments were performed mainly on systems exhibiting positive dielectric anisotropy  $\Delta\epsilon = \epsilon_{\parallel} - \epsilon_{\perp}$ , where the subscripts refer to directions in relation to  $\hat{n}$ . The dielectric anisotropy is a measure of the order parameter  $S \simeq \Delta\epsilon / \Delta\epsilon_a$ , where  $\Delta\epsilon_a$  is the dielectric anisotropy in the fully aligned state.  $\Delta\epsilon$  couples with  $E^2$  to lower the free energy density:  $F_E = -(\epsilon_0 \Delta\epsilon_a S E^2) / 2$  where  $E$  is the applied electric field and  $\epsilon_0$  the vacuum dielectric constant. The field induces a weak orientational order even in the isotropic phase (*paranematic*), as a result of which all the physical properties in the medium become weakly anisotropic. The field-induced birefringence ( $\Delta n$ ) in the paranematic phase due to the electric field is called the Kerr effect, and the analogous effect due to a magnetic field is called the Cotton-Moutton effect. Under the action of the field the paranematic to nematic transition temperature is shifted towards higher values and the order parameter is increased in the nematic phase also. At low fields the transition occurs with a finite jump in the order parameter in a first order phase transition. With increasing field the jump decreases and above the critical field there is a continuous evolution of the order parameter from paranematic to nematic phase in materials with  $\Delta\epsilon > 0$ . The symmetries of the two phases are the same and the

<sup>a</sup> e-mail: sdsp@uohyd.ernet.in

<sup>b</sup> e-mail: nvmadhu@rri.res.in

possibility of a second order phase transition can be ruled out. These phenomena resemble the classical liquid to gas transition under pressure [2]. To shift the transition temperature by a measurable quantity the electric or the magnetic free energy per molecule should be comparable to the thermal energy  $k_B T$ . The volume diamagnetic susceptibility anisotropy of a typical nematic is  $10^{-6}$  m<sup>3</sup>/mol, and the required magnetic field is  $10^3$  tesla, which is beyond experimental realization. On the other hand materials with large positive dielectric anisotropy of  $\sim 20$  are available and the required electric field is approximately  $10^7$  V/m and attainable in the laboratory. If  $\Delta\epsilon > 0$ , the director is aligned along the direction of the applied electric field and the enhancement in the order parameter is due to the Kerr effect as well as quenching of director fluctuations but the system remains uniaxial [2]. Studies on the effect of strong electric fields on liquid crystals with negative dielectric anisotropy are also interesting because the phase diagram is very different in nature compared to that in a system with  $\Delta\epsilon > 0$ . A strong dipolar group which makes a large angle with the long axis of the molecule is needed to get a material with  $\Delta\epsilon < 0$ . To study the electric field effect, the nematic liquid crystal is sandwiched between two ITO (indium-tin oxide) coated glass plates, which are treated for planar alignment of  $\hat{n}$  along the  $X$ -axis. The field is applied along the  $Z$ -axis as shown in Figure 1a. The dipoles of the molecules tend to align along the field direction. As a result the long molecular axes tend to be perpendicular to the field direction. In the paranematic phase the distribution of azimuthal angles of the molecules in the  $(XY)$  plane perpendicular to the field is random. The projections of the long axes of the molecules in the  $XY$  plane are also shown in Figure 1a. The distribution function  $f(\theta)$  of the long axes around the field direction shows a small peak at  $\theta = \pi/2$ . With increasing field the peak height increases as schematically shown in Figure 1b. The paranematic phase ( $N_{U^-}$ ) is uniaxial with a *negative* order parameter. When the system is cooled under the field below the paranematic to nematic transition temperature the long axes of the molecules tend to align in a preferred direction ( $X$ -axis say) which can be controlled by the surface interaction with the treated plates. In the nematic phase there is a partial quenching of the director fluctuations due to the electric field in the  $ZX$  plane. Thus the fluctuations in the  $ZX$  plane are smaller than those in the plane  $(XY)$  perpendicular to the field as shown in Figure 1a. The differential quenching of fluctuations leads to induced biaxiality under field [3, 10]. Therefore, under the field the paranematic to nematic transition corresponds to uniaxial nematic ( $N_{U^-}$ ) to biaxial nematic ( $N_B$ ) transition. With increasing field the  $N_{U^-}$  to  $N_B$  transition temperature is shifted to higher values and the order parameter (see Eq. (1) in Sect. 2) is increased in the  $N_B$  phase. The jump in the order parameter reduces and finally the transition between the two phases with different symmetries becomes second order in nature above the tricritical field.

The main problem in conducting high electric field experiments on liquid crystals is the heating due to ionic

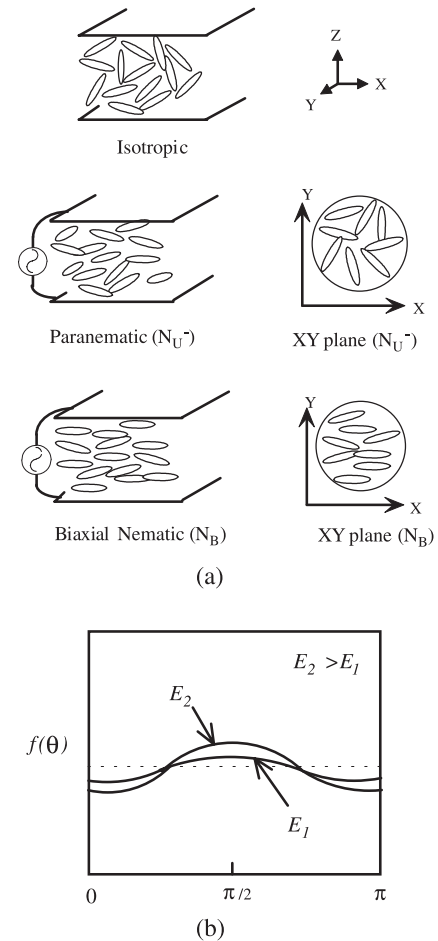


**Fig. 1.** (a) Schematic representation of the distribution of molecules in the field induced paranematic ( $N_{U^-}$ ) and biaxial nematic ( $N_B$ ) liquid crystals with  $\Delta\epsilon < 0$ . The relative sizes of the molecules are exaggerated for clarity. (b) Schematic representation of the distribution function in the presence of electric field above  $T_{PN}$ . Dotted line represents the distribution function without field in the isotropic phase, and the continuous line that in the paranematic phase with applied field. The peak around  $\pi/2$  is exaggerated for clarity.

conductivity of the sample as well as dielectric relaxation. There can also be a hydrodynamic instability [1] for systems with  $\Delta\epsilon < 0$ . The first qualitative observation of the critical field for a positive  $\Delta\epsilon$  material was due to Nicastro and Keyes [4] who used a DC external field. They also measured the DC Kerr effect in the isotropic phase of a negative  $\Delta\epsilon$  material. To minimise the heating effect Durand et al. [5, 6] applied an electric field of short pulse width ( $\sim 10$  to  $100 \mu s$ ) with long off period i.e. with a small duty cycle. In this technique it takes a long time ( $\sim 40$  min) to collect each data point. We have adapted a technique developed by Basappa et al. [7]. In this, the *local temperature* of the sample is measured under field and the data points are collected continuously. This technique enables us to perform optical as well as electrical measurements simultaneously on materials with  $\Delta\epsilon < 0$ .

In this paper we report the following results on a material with  $\Delta\epsilon < 0$ : (a) electric field induced enhancement of birefringence in the nematic phase, (b) dielectric measurement of the field induced order in the paranematic phase, (c) an essentially *linear* dependence of the uniaxial paranematic to biaxial nematic transition temperature on the modulus of the field, (d) divergence of the order parameter susceptibility above the tricritical point as measured by 3rd harmonic electrical signal and (e) detection of a small 2nd harmonic electrical signal at a high field. The result (c) has already been reported in a brief letter [11].

## 2 Theoretical background

The application of an external electric field to a nematic liquid crystal with a negative dielectric anisotropy induces biaxial ordering. Considering up to the fourth order term in the expansion, the Landau de Gennes free energy in the presence of an external electrical field can be written as [2,3]

$$F = -\frac{\epsilon_o}{2}\Delta\epsilon_a E_\alpha E_\beta Q_{\alpha\beta} + \frac{1}{2}A' TrQ^2 + \frac{1}{3}B' TrQ^3 + \frac{1}{4}C' (TrQ^2)^2 \quad (1)$$

where  $Q$  is the tensor order parameter and  $A' (=a'(T - T^*))$ ,  $B'$ ,  $C'$  are Landau coefficients and  $T^*$  the lowest supercooling limit of the isotropic phase. The tensor order parameter can be defined as

$$Q_{\alpha\beta} = \begin{pmatrix} -\frac{1}{2}(x+y) & 0 & 0 \\ 0 & -\frac{1}{2}(x-y) & 0 \\ 0 & 0 & x \end{pmatrix} \quad (2)$$

where  $x$  is related to  $S$  defined earlier ( $x = 2/3S$ ) and  $y$  is the biaxial order parameter which distinguishes between two directions orthogonal to the director. The equilibrium order parameters can be found by minimising the free energy density  $F$ . The calculated phase diagram using this model for a nematic liquid crystal with negative dielectric anisotropy is schematically shown in Figure 2 in which  $h = \epsilon_o \Delta\epsilon_a E^2/3$ . The dependence of  $T_{PN}$  on field can be expressed analytically only when it becomes *second ordered*, above the tricritical point. At such high fields,  $\Delta T = T_{PN} - T_{NI}$  where  $T_{NI}$  is the field free isotropic to nematic transition point, is found to depend both on  $|E|$  as well as  $E^2$  [2,3]. However, as discussed in reference [3], at lower fields, the *first order* transition point can only be calculated numerically.  $\Delta T$  has a practically linear dependence on  $E^2$  [1,3] as shown schematically in Figure 2. For small  $E$  values,  $\Delta T$  and  $\Delta x = x(E) - x(0)$ , the change in the order parameter in the nematic phase at the transition point are also small. Expanding the free energy to linear order in  $\Delta x$  and  $\Delta T$ , it can be shown that  $\Delta T \propto E^2$ .

## 3 Experimental

In order to measure the local temperature of the sample we use an evaporated nickel (Ni) film to design a tem-

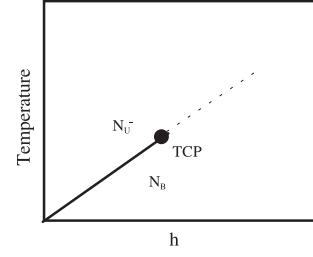


**Fig. 2.** Schematic representation of the  $h(\propto E^2)$ ,  $T$  phase diagram of a nematic with  $\Delta\epsilon < 0$ . Thick line indicates first order transitions, and dashed line second order transitions: TCP denotes the tricritical point. (adapted from Ref. [2])

perature sensor. Ni shows high temperature coefficient of resistance ( $\sim 6180$  ppm/K). A thin film of nickel is vacuum coated on a plane glass plate. A zigzag pattern of the nickel film, which has a strip width  $\sim 200 \mu\text{m}$  and total length  $\sim 0.05$  m is etched using a photolithographic technique. The resistance of the pattern is  $\sim 100$  to  $200 \Omega$ . The Ni thermometer is calibrated in each individual cell. The thermometer is covered with a thin layer of insulating SiO on which a circular aluminum (Al) electrode ( $0.5$  cm diameter) is vacuum evaporated. In order to reduce the field gradient at the edge, a guard ring is provided just outside the Al electrode with separation of  $100 \mu\text{m}$  as shown in Figure 3a. The top electrode is an ITO coated glass plate. Finally a thin layer of SiO is coated on both the plates at a grazing angle of  $30^\circ$  using a vacuum evaporation technique. The director is aligned orthogonal to incident direction of the SiO beam [1]. Mylar spacers are used to obtain the required cell thickness. The sample thickness is measured outside the electrode area by an interferometric technique. The typical cell thickness is  $\sim 16 \mu\text{m}$ . The electrical connections to the two plates are made through copper wires which are soldered using an ultrasonic soldering gun. The cross section of a typical cell is schematically shown in Figure 3b. The cell is mounted in an Instec hot-stage (HS1) which itself is placed on the rotating stage of a microscope (Leitz, Orthoplan). The temperature is controlled to an accuracy of  $0.008^\circ\text{C}$ . The cells are filled with the sample in the isotropic phase and on slow cooling to the nematic range, well-aligned samples are obtained.

The block diagram of the experimental set up is shown in Figure 4. The output voltage of a lock in amplifier (LIA, model SRS 830) is connected to a high gain voltage amplifier (TREK, 601-2). The output of the amplifier is connected to one of the two branches as shown in Figure 4. In one branch there is a potential divider circuit, which is made of two resistors ( $100 \Omega$  and  $1 \text{ M}\Omega$ ) connected in series. The potential divider circuit is used to measure the phase and amplitude of the amplified voltage. In another branch the sample cell is connected in series with a capacitor  $C_m$  ( $\sim 1 \mu\text{F}$ ). A manual DPDT switch is used to switch between the two branches. The signal across the capacitor  $C_m$  is used to measure the phase and amplitude of the current flowing in the cell. Using an impedance analysis technique [7] we measure the capacitance ( $C_S$ ) and resistance ( $R_S$ ) of the sample. If  $V_0$  and  $\phi_0$  are the amplitude

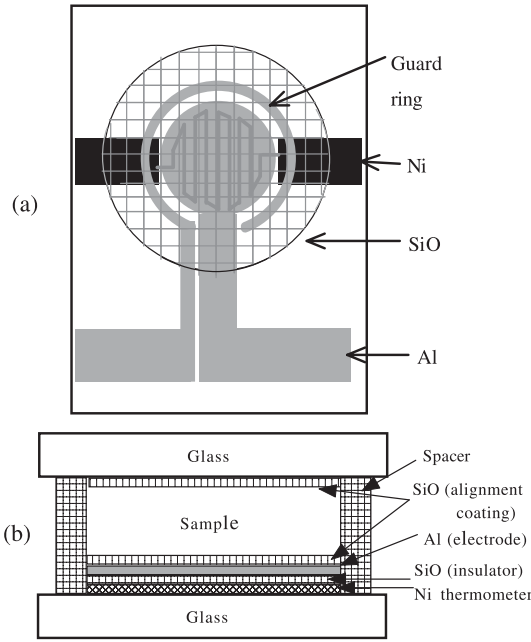


**Fig. 3.** (a) Schematic diagram of the structure of the lower electrode. There is an insulating SiO coating between Ni thermometer and the Al electrode. Note the zigzag pattern of the Ni thermometer. (b) Schematic of the side view of the cell (not to scale).

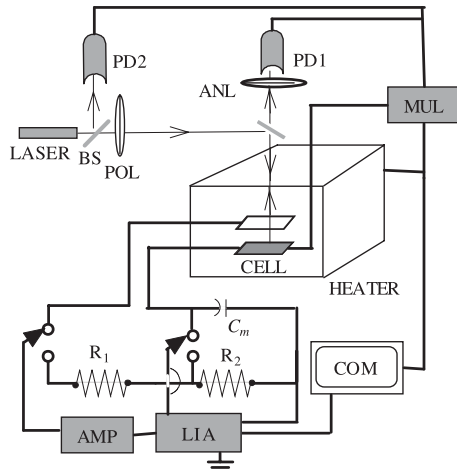


**Fig. 4.** Schematic diagram of the experimental setup. PD1, PD2 (Photodiodes). POL (Polariser), ANL (Analyser), MUL (Multimeter), AMP (Voltage Amplifier), LIA (Lock in amplifier),  $R_1$ ,  $R_2$  (Resistances), COM (Computer).

and phase at the output of the amplifier and  $V_m$  and  $\phi_m$  are those measured across the capacitor  $C_m$ , it can be shown that the capacitance and resistance of the sample are given by [7]:  $R_S = Y/(\omega \sin \alpha)$ ,  $C_S = X/Y$  where  $X = \cos \alpha - Q$ ,  $Y = (\sin^2 \alpha + X^2)/(C_m Q)$ ,  $Q = V_m/V_o$ ,  $\alpha = \phi_o - \psi_m$  and  $\omega = 2\pi f$ ,  $f$  is the frequency of the applied signal. The dielectric constant of the sample is given by  $C_S/C_o$ , where  $C_o$  is the capacitance of the empty cell.

The lower electrode is opaque due to the Al and Ni coatings, and it is not possible to perform optical mea-

surements in the transmission mode. As we have used an ITO coated glass plate as the top electrode, the optical measurements can be made in the reflection mode of the microscope. A laser beam (He-Ne,  $\lambda = 632.8$  nm) is passed through a polariser (POL) and made to be incident on the sample. The bottom Al electrode reflects the laser beam. The reflected beam is passed through an analyser (ANL) which is crossed with respect to the polariser. A photodiode (PD1, model Centronics OSD-5) is used to measure the reflected intensity. The stability of the laser intensity is monitored by another photodiode (PD2). A multimeter (MUL, Keithley 2000) is used to measure the output voltages of both the photodiodes as well as the resistance of the Ni thermometer. The temperature variation of the optical intensity is measured. The intensity in this geometry is given by the relation

$$I = \frac{\sin^2 2\psi}{2} (1 - \cos \Delta\phi) \quad (3)$$

where  $\psi$  is the angle made by the polariser with the optic axis and the phase difference

$$\Delta\phi = \frac{2\pi}{\lambda} \Delta n 2d \quad (4)$$

where  $\Delta n = n_e - n_o$ ,  $n_e$  and  $n_o$  are the extraordinary and ordinary refractive indices of the liquid crystal medium.  $d$  is the sample thickness and the factor 2 arises because the light travels twice across the sample thickness in the reflection mode. The angle  $\psi$  is set at  $45^\circ$  to optimise the measurements. The birefringence is calculated from the measured intensity. The frequencies and the voltage ranges used in the experiments are 4111, 15111 Hz, and 5 to 270 V respectively. The sample used is 4'-butyl-4 heptyl-bicyclohexyl-4-carbonitrile (CCN47) obtained from Merck. It has the following phase transitions: Cr 28 °C SmA 30.6 °C N 59.7 °C I. This compound exhibits room temperature liquid crystalline phase with a large negative dielectric anisotropy ( $-8.0$  at 20 °C). The measurements are completely controlled by a computer, using a suitable program. All the experiments are performed on cooling the sample from the paranematic phase.

## 4 Results and discussion

Variations of birefringence ( $\Delta n$ ) as well as dielectric constant ( $\epsilon_{\perp}$ ) are shown as functions of local temperature (measured by the Ni resistance thermometer) at various fields in Figures 5a and 5b respectively. The following important features are noted from Figure 5a: (i) with increasing field (a)  $\Delta n$  is enhanced in the nematic phase and (b) the paranematic to nematic ( $N_{U^-} - N_B$ ) transition temperature ( $T_{PN}$ ) is shifted toward higher values; (ii)  $\Delta n$  rises from zero relatively sharply as the temperature is lowered in the phase transition region; (iii) separations among the curves are quite wide close to the transition point and are reduced as the temperature is lowered in the nematic phase. The experiments were conducted on

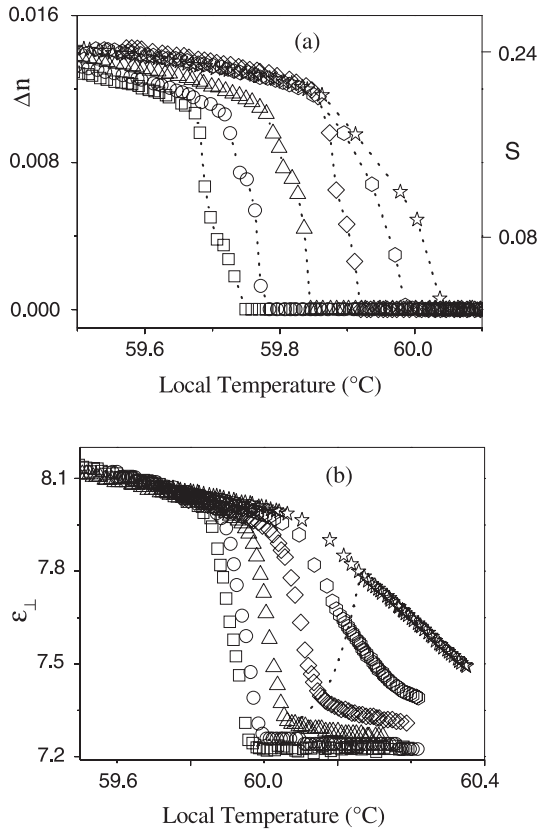


**Fig. 5.** (a) Variations of  $\Delta n$  as well as  $S$  across the paranematic-nematic transition region as functions of local temperature at  $1.5 \times 10^5$  V/m (squares),  $3.3 \times 10^6$  V/m (circles),  $6.5 \times 10^6$  V/m (triangles),  $9.8 \times 10^6$  V/m (diamonds),  $1.3 \times 10^7$  V/m (hexagons),  $1.6 \times 10^7$  V/m (stars). Frequency of the applied field: 4111 Hz. Cell thickness:  $16.4 \mu\text{m}$ . (b) Variation of  $\epsilon_{\perp}$  across the paranematic-nematic transition region as a function of local temperature at the same fields measured simultaneously with  $\Delta n$  shown in (a). Dotted line connects the temperatures (designated as  $T_{PN}$ ) at which the  $\Delta n$  starts to rise from zero value.

three independent samples and the results are similar in all the cases.

The temperature at which  $\Delta n$  starts rising from zero value is a measure of the paranematic to nematic transition temperature ( $T_{PN}$ ). At low fields, the paranematic to nematic transition is first ordered in nature, and one would expect a sharp jump in the birefringence at  $T_{PN}$ . In our experiments, the temperature resolution is 8 mK, and as can be seen from Figure 5a, the width of the transition region is  $\leq 0.06$  K, for fields upto  $9.75 \times 10^6$  V/m. The width is similar for the four curves, which implies that it does not arise from field gradients within the area of illumination by the laser beam. The width may partly arise from dissolved impurities. Adiabatic calorimetric measurements have shown that even a highly stable low temperature nematogen like hexyl cyanobiphenyl exhibits a two phase co-existence of 30 mK around  $T_{NI}$  [12]. An additional contribution to the width can arise from the nature of our experiment. The transmitted intensity acquires a nonzero value

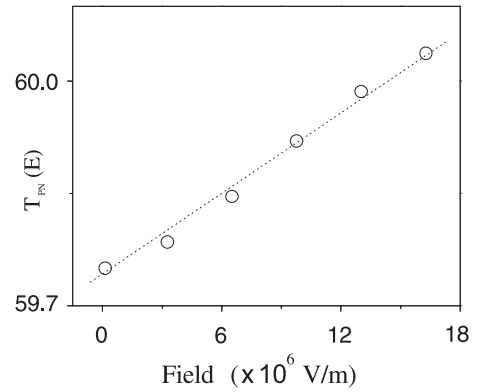


**Fig. 6.** Variation of paranematic-nematic transition temperature ( $T_{PN}$ ) as a function of applied field. Data points are obtained from the results shown in Figure 5a.

as soon as there is some alignment along the  $x$ -axis. The alignment naturally is initiated at the two treated surfaces of the  $16 \mu\text{m}$  thick cell. The alignment can be expected to pervade the entire cell at a slightly lower temperature, which should be considered as the true bulk paranematic to nematic transition point. In any case, as all the experimental runs have been made under similar conditions on cooling the sample, the *relative* shifts should not be sensitive to the method of identifying the transition temperature. The well separated temperatures at which the birefringence becomes nonzero can be taken as a measure of  $T_{PN}$ .

The variation of  $T_{PN}$  obtained from Figure 5a is shown as a function of field in Figure 6. A large shift in  $T_{PN}$  ( $\sim 0.3^\circ$ ) is measured between  $1.5 \times 10^5$  to  $1.6 \times 10^7$  V/m. The important result is that  $T_{PN}$  varies *linearly* with the rms field. It may be recalled that a *quadratic* variation of  $T_{PN}$  is predicted by the Landau de Gennes free energy as shown in Figure 2. This has to be contrasted with the clearly quadratic dependence of the shift in the smectic A-nematic (AN) transition point with field in the case of octyloxy cyanobiphenyl [7]. The linear variation of  $T_{PN}$  as a function of field indicates that the quenching of director fluctuations not only increases the order parameter but also has a strong influence on the phase transition. This point was not recognised in earlier high electric field experiments on systems with  $\Delta\epsilon > 0$  [5]. In the case of AN transition, both bend and twist elastic constants diverge as the transition point is approached from the nematic side, and correspondingly, the director fluctuations tend to zero and thus do not influence the thermodynamics of the transition. It should be mentioned that on prolonged application of high fields the sample degraded slightly reducing the nematic to isotropic transition temperature. We have carried out experiments only for a few fields to complete the experiment quickly (in  $\sim 8$  h) and hence avoided such degradation.

In the nematic phase, for example at  $59.6^\circ\text{C}$  (see Fig. 5a) the enhancement in  $\Delta n$  is measurable up to  $\sim 9.75 \times 10^6$  V/m. Beyond that the curves in the nematic phase are crowded though they are well separated in the transition region. Visual observations of the sample were

made between crossed polarisers in the nematic phase with the principal director oriented parallel to the polariser (see Fig. 4). Up to a field of  $\sim 1.1 \times 10^7$  V/m, the field of view is uniformly dark. Beyond this field, some birefringent regions are seen along with the motion of some dust particles. In spite of using a guard ring there may be a field gradient at the edges of the sample. The field may also be nonuniform inside the cell due to slight variations of the local thickness or the presence of the dust particles in the sample. Such field gradients which may not be in the region in which the laser beam is incident can cause physical motion of the medium at high fields. As a result the sample can get misaligned and lead to light transmission. The merging of the curves beyond  $10^7$  V/m probably occurs due to such a misalignment.

From the dielectric data (shown in Fig. 5b) several important points can be noted: the width of the transition is somewhat larger than that found in the optical experiments. The increase of the paranematic to nematic transition temperature with field is however seen clearly. The temperatures which are connected by a dotted line in Figure 5b are obtained from Figure 5a and correspond to those at which  $\Delta n$  starts to rise from zero. The larger width of the transition may arise due to the fact that  $\epsilon_{\perp}$  is measured over a large area ( $2 \times 10^{-5}$  m<sup>2</sup>) over which the temperature may have some nonuniformity. With increasing field,  $\epsilon_{\perp}$  is increased in the  $N_U$ - phase (see right side of the dotted line in Fig. 5b). This shows that the induced order parameter is also increased. We can calculate the uniaxial negative order parameter in the paranematic phase from the dielectric data, which will be discussed later. At temperatures well below the transition region  $\epsilon_{\perp}$  decreases slowly with decreasing temperature and the enhancement of  $\epsilon_{\perp}$  with increasing field is also very small. On the other hand, with increasing field a substantial enhancement of  $\Delta n$  which is directly proportional to  $S$  is observed well below the transition temperatures also.

The orientational order parameter for uniaxial nematic liquid crystals can be well approximated by  $S \approx \Delta n / \Delta n_0$ . The birefringence of the compound used is very small, and hence the internal field corrections are negligible. Thus it is a legitimate approximation to calculate the order parameter directly from  $\Delta n$  data. In the nematic phase under an electric field (as  $\Delta \epsilon < 0$ ) the director fluctuations in the plane containing the field are reduced compared to those in the orthogonal plane. As a result the system becomes biaxial, which is described by the order parameter  $S$  and the biaxial order parameter  $P$ , which is related to  $y$  (see Eq. (2)). In our experiment we measure the birefringence in the plane orthogonal to the electric field. This is a measure of  $(S - P)$  rather than  $S$ . However, the field induced biaxial order parameter  $P \sim 10^{-3}$  (at  $\sim 3 \times 10^6$  V/m) in a similar sample [10] whereas  $S \sim 0.2$ . Hence we use  $\Delta n$  as a measure of the order parameter  $S$ . We have measured  $\Delta n$  over the entire nematic range of the field free sample to estimate  $\Delta n_0$ , the value for perfect orientational order ( $S = 1$ ) by using the Haller extrapolation procedure [13]. The scale corresponding to  $S = \Delta n / \Delta n_0$  is also marked in Figure 5a. The Landau de Gennes theory [1] gives rise to

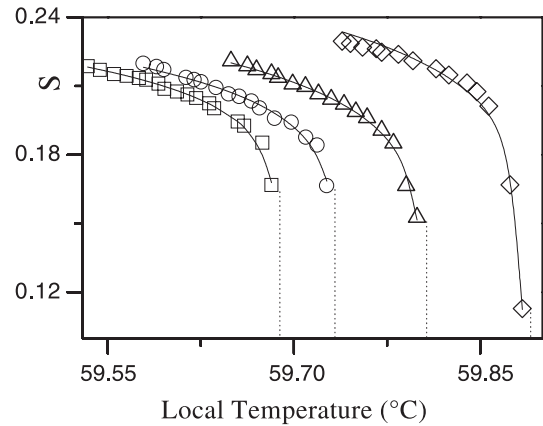


**Fig. 7.** Variations of order parameter at different fields in the nematic phase within  $0.15^\circ\text{C}$  of the transition point. Continuous lines are the theoretical fits to equation (5). Vertical dotted lines indicate the temperatures corresponding to the fitted values of  $T^{**}$ .

the following form of the temperature dependence of the order parameter in the field free uniaxial nematic liquid crystal:

$$S - S_0 = \alpha \left(1 - \frac{T}{T^{**}}\right)^\beta \quad (5)$$

where  $T^{**}$  is the absolute limit of superheating of the nematic phase,  $S_0$  is the order parameter at  $T^{**}$ ,  $\beta = 0.5$ , and  $\alpha$  is a proportionality constant.

According to the Landau de Gennes theory [1] ( $T^{**} - T_{NI}$ ) is 8 times smaller than  $(T_{NI} - T^*)$ . Experiments show that  $T^* \sim T_{NI} - 1$ . Thus  $T^{**}$  is  $\sim 0.1^\circ$  above  $T_{NI}$ , according to the theory. As is well known [1] experimental results on most nematogens yield  $\beta \approx 0.2$ , which reflects the inadequacy of the meanfield model. In our samples there is a small width of the paranematic to nematic transition. We can fit the temperature variation of the order parameter by treating equation (5) as an *empirical relation* which is valid even in the presence of the field. The field dependence of  $T^{**}$  can be expected to reflect the variation of the *bulk* transition temperature. We use the data in the nematic phase within only  $0.15^\circ\text{C}$  from the transition point in this analysis. As we have mentioned, there is some misalignment of the sample beyond  $\sim 10^7$  V/m and hence we will consider the order parameter data only up to  $9.75 \times 10^6$  V/m. In Figure 7 experimental values of the order parameter in the nematic phase within  $0.15^\circ\text{C}$  from the transition point as well as the calculated variations using equation (5) are shown. The comparison between the two is reasonably good up to  $6.5 \times 10^6$  V/m, and not so good for  $9.75 \times 10^6$  V/m. The fitted values of  $S_0$ ,  $\alpha$ ,  $\beta$  and  $T^{**}$  are shown in Table 1.  $T^{**}$  at different fields are also indicated by vertical dotted lines in Figure 7. The values of  $T_{PN}$  which are defined as the temperature below which the birefringence becomes nonzero (see Fig. 5a) are also shown in Table 1 to compare with  $T^{**}$ . From Table 1 it is seen that  $T^{**}$  is  $\sim 0.07^\circ\text{C}$  lower than  $T_{PN}$  at  $1.5 \times 10^5$  V/m and the difference is reduced to  $0.04^\circ\text{C}$  at a field of  $9.75 \times 10^6$  V/m. This small difference between  $T^{**}$

**Table 1.** Parameters which fit equation (5) at different fields.

Field in V/m	$S_0$	$\alpha$	$\beta$	$T^{**}$ ( $^{\circ}\text{C}$ )	$T_{PN}$ ( $^{\circ}\text{C}$ )
$1.5 \times 10^5$	0.12	0.37	0.17	59.68	59.75
$3.27 \times 10^6$	0.11	0.40	0.17	59.73	59.78
$8.51 \times 10^6$	0.09	0.47	0.17	59.80	59.86
$9.75 \times 10^6$	0.08	0.52	0.16	59.88	59.92

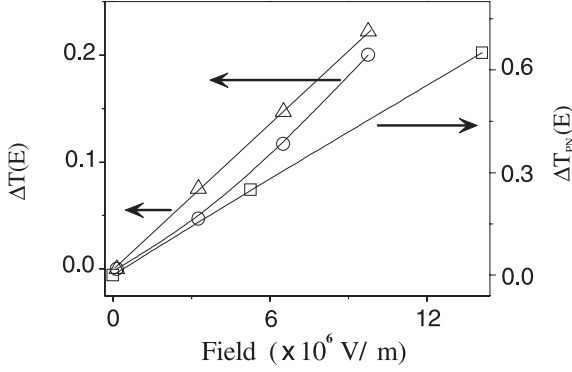


**Fig. 8.** Dependence on electric field of  $\Delta T_{PN} = (T_{PN}(E) - T_{NI}(0))$  (triangles), where  $T_{PN}(E)$  is the temperature at which the birefringence starts to rise from zero (see Fig. 5a), and of  $\Delta T^{**} = T^{**}(E) - T^{**}(0)$  (circles, see Fig. 7). Variation of  $\Delta T_{PN}$  (squares) of 5CB obtained from Figure 3 of reference [5] is also shown.

and  $T_{PN}$  is a measure of the width of the transition, discussed earlier. When the field is increased from  $\sim 1.5 \times 10^5$  to  $\sim 9.75 \times 10^6$  V/m,  $S_0$  decreases from 0.12 to 0.08, indicating that the strength of the transition is decreased as the field is increased as expected. The value of  $\beta$  is almost constant (0.17) and decreases slightly to 0.16 at  $9.75 \times 10^6$  V/m. In order to measure  $\epsilon_{\perp}$ , the lowest field applied was  $1.5 \times 10^5$  V/m. As the field is too small to cause any measurable change in the properties near  $T_{NI}$ , we assume that  $T^{**}$  for  $1.5 \times 10^5$  V/m is  $T^{**}(0)$ . The field variation of  $\Delta T^{**} (= T^{**}(E) - T^{**}(0))$  is shown in Figure 8. The amount of shift is  $\sim 0.2$   $^{\circ}\text{C}$  which is similar to the shift of  $\Delta T_{PN}$  when the field is increased from  $1.5 \times 10^5$  V/m to  $9.75 \times 10^6$  V/m. The important observation is that the variation of  $\Delta T^{**}$  is essentially linear with  $|E|$ . The electric field phase diagram of a nematogen with  $\Delta\epsilon > 0$  has been published [5]. However,  $\Delta T_{PN} (= T_{PN}(E) - T_{NI}(0))$  has not been plotted as a function of  $|E|$  in this study. We use the data given in Figure 3 of reference [5] and plot the shift  $\Delta T_{PN}$  of pentyl cyanobiphenyl (5CB) also in Figure 8. It is clear that  $\Delta T_{PN}$  shifts *linearly* with  $|E|$  in this case as well.

#### 4.1 Order parameter enhancement by the field

*Nematic Phase.* The increase in order parameter due to the application of electric field arises because of two physical mechanisms. One mechanism is the macroscopic quenching of thermal fluctuations of the director [1]. As in the case of materials with  $\Delta\epsilon > 0$  [6] the enhancement of order parameter for a system with  $\Delta\epsilon < 0$  due to this

effect alone can be written as

$$\begin{aligned} \delta S_l &= S(E, T) - S(0, T) = \frac{3K_B T}{8\pi(K)^{3/2}} (\epsilon_o \Delta\epsilon)^{1/2} |E| \\ &= C_l |E| \end{aligned} \quad (6)$$

where  $K$  is the average curvature elastic constant,  $S(E, T)$  is the order parameter in the presence of field and  $S(0, T)$  is the same in the absence of field at the temperature  $T$ . The subscript  $l$  indicates a *linear* variation with  $|E|$ . The electric field quenches director fluctuations only in the plane containing the field. The fluctuation components in the orthogonal plane are not quenched, and as such the numerical value of  $C_l$  is smaller than in materials with positive  $\Delta\epsilon$  [1]. In the mean field approximation  $K \propto S^2$ , and as  $\Delta\epsilon \propto S$ ,  $C_l \propto S^{-5/2}$ . As we shall see below, close to the NI transition point, the variation of  $C_l$  is much steeper, and we can write  $C_l \propto S^{-x}$ , in general. As discussed by Lelidis et al. [6], the enhancement of the order parameter due to the quenching of thermal fluctuations in turn generates a saturating term in second order, which is given by:

$$\delta S_{lq} = C_{lq} E^2 = -x \frac{C_l^2}{S(0)} E^2 \quad (7)$$

The other mechanism for the enhancement of order parameter under the application of field is the Kerr effect, which is microscopic in origin. The increase in order parameter due to this effect alone can be written as

$$\delta S_{kq} = C_{kq} E^2 \quad (8)$$

where  $C_{kq}$  is an appropriate susceptibility. This effect is *quadratic* in  $E$ , indicated by the subscript  $q$ . The enhancement in the order parameter due to both the effects can be written as

$$\delta S(E) = \delta S_l + \delta S_q = C_l |E| - x \frac{C_l^2 E^2}{S(0)} + C_{kq} E^2 \quad (9)$$

The variations of measured  $\delta S(E) (= S(E) - S(0))$  at different temperatures very close to  $T_{NI}$  are shown in Figure 9a. Using a least squares fitting procedure, the enhancement of the order parameter is fitted with equation (9). The temperature variations of the fitted parameters  $C_l$  and  $C_q (= C_{lq} + C_{kq})$  are shown in Figure 9b.  $C_l$  decreases and  $C_q$  increases as the temperature is lowered in the nematic phase [6, 8]. The measurements which have been made within  $\sim 0.2$   $^{\circ}\text{C}$  of  $T_{NI}$  show that  $x \simeq 5$ , which is much larger than the mean field value of 5/2. The rapid increase of  $C_l$  as the temperature is increased leads to an even more rapid increase in the negative contribution to the quadratic term as given in equation (9). Thus, though  $C_{kq}$  also increases with temperature, the contribution from the quenching of fluctuations dominates, and leads to a lowering of the net  $C_q$  as  $T_{NI}$  is approached. The overall field induced enhancement of the order parameter of course increases as  $T_{NI}$  is approached and is dominated by  $\delta S_l$ .

*Paranematic Phase.* In the field induced paranematic phase the symmetry axis is parallel to the laser beam and

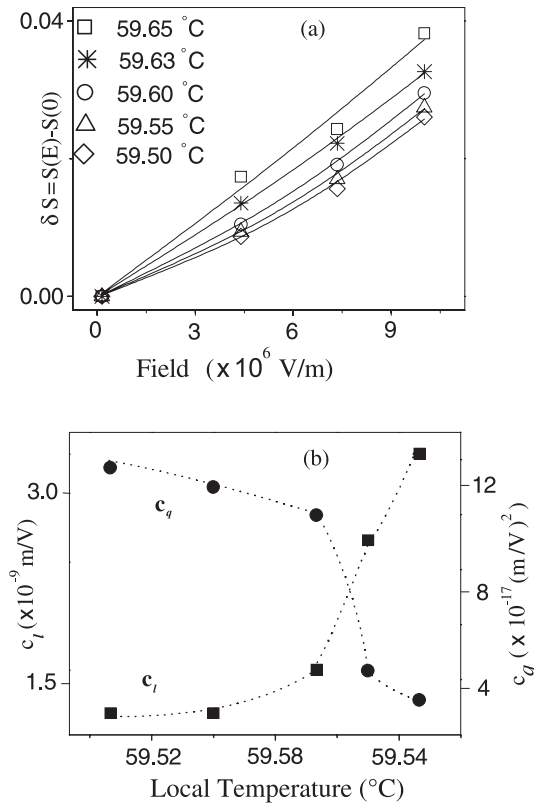


**Fig. 9.** (a) Variation of enhancement of the order parameter ( $\delta S$ ) as a function of field at different local temperatures. Continuous lines are fit to the functional form of  $\delta S = C_l|E| + C_qE^2$ . (b) Variations of the fitted parameters,  $C_l$  and  $C_q$  as functions of local temperature. Dotted lines are drawn as guides to the eye.

therefore we can not measure the order parameter using the optical technique. However we can calculate the uniaxial negative order parameter ( $S_{U-}$ ) from the dielectric data taken from Figure 5b. Thus the measurement yields  $\epsilon_{||}^P = \bar{\epsilon} + \frac{2}{3}\Delta\epsilon_a S_{U-}$  where the superscript signifies paranematic phase and the subscript refers to the direction which is parallel to the symmetry axis. On the other hand, in the nematic phase the principal director is perpendicular to the field and we measure  $\epsilon_{\perp}^N$  which is given by  $\epsilon_{\perp}^N = \bar{\epsilon} - \Delta\epsilon_a S/3$ , ignoring biaxiality which is very small. (Above the tricritical point the paranematic-nematic transition is second order and,  $\epsilon_{||}^P = \epsilon_{\perp}^N$  and hence it is expected that  $S_{U-} = -S/2$  at  $T_{PN}$ .) We have used  $\epsilon_{\perp}$  at  $1.5 \times 10^5$  V/m and the value of  $S$  obtained by optical measurement at  $(T_{PN} - 2)$  °C to evaluate  $\Delta\epsilon_a = -9.97$ . The variation of uniaxial order parameter  $S_{U-}$  is shown as a function of the applied field at  $T = 60.1$  °C in Figure 10. The enhancement of order parameter in the paranematic phase arises mainly due to the Kerr effect and we use a least squares fitting procedure to fit the data with the equation  $S = C_q E^2$ . The agreement with the measured data is not very good. As we discussed earlier the dielectric constant is measured over a large area ( $2 \times 10^{-5}$  m<sup>2</sup>) and the field and temperature may not be uniform in the

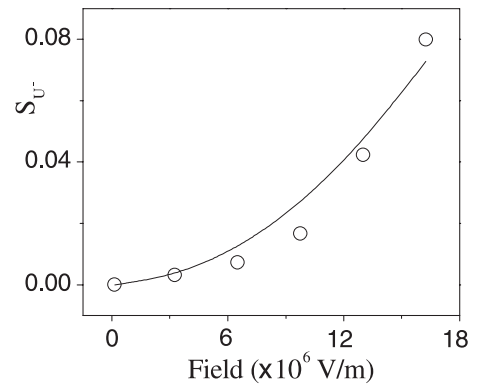


**Fig. 10.** Variation of uniaxial negative order parameter ( $S_{U-}$ ) in the paranematic phase as a function of applied field at a temperature 60.1 °C. Circles are experimental data. Continuous line is the fit to the functional form  $S = C_q E^2$ , where  $C_q = 2.8 \times 10^{-16}$  (m/V)<sup>2</sup>.

cell. The fit parameter  $C_{kq} = 2.8 \times 10^{-16}$  (m/V)<sup>2</sup> and is comparable to the value of  $C_{kq}$  in the nematic phase.

#### 4.2 Variation of paranematic to nematic transition point with field: influence of director fluctuations

As shown in Figure 8,  $T_{PN}$  as well as  $T^{**}$  vary linearly with  $|E|$ . This is true for systems with both  $\Delta\epsilon > 0$  as well as  $\Delta\epsilon < 0$ . This clearly shows the importance of the quenching of director fluctuations even in the thermodynamics of the paranematic to nematic (PN) transition under electric fields.

We may point out an analogous problem of the undulation interaction, which arises in lamellar systems. In this case, the layer fluctuations are restricted due to the presence of the neighbouring layers and the corresponding increase in the free energy was calculated by Helfrich [15]. In the case of nematic liquid crystals the amplitudes of the director fluctuations are reduced in the presence of the field. We can use a dimensional analysis to estimate the corresponding increase in the free energy density. Our experiments were conducted on samples of  $\sim 16$   $\mu\text{m}$  thickness. Theoretical calculations [10,16] show that at such a thickness, the director fluctuations are not significantly suppressed by the boundary conditions. However, Dummur et al. [10] found that the measured quenching of fluctuations by an external electric field is significantly smaller than the theoretical estimate for a sample of thickness of  $\sim 12$   $\mu\text{m}$ . We have not carried out measurements on the thickness dependence of the electric field effects. Our earlier studies have shown that in the absence of external fields, there is a significant increase in the measured order parameter when the sample thickness is reduced to a much smaller value,  $\sim 1$   $\mu\text{m}$  [16], implying a strong suppression of the fluctuations in the latter case. We do not consider the influence of the sample boundaries in the following analysis of the electric field effects. There are two important length scales in this problem. One is the electric coherence length  $\xi(E) = \left(\frac{K}{\epsilon_o \Delta\epsilon}\right)^{\frac{1}{2}} \frac{1}{|E|}$ , which is

a length such that the director fluctuations with wavelengths longer than  $\xi$  are essentially suppressed by the field [1]. The other length gives rise to the cut off wave vector  $q_c = 2\pi/l$ , for the applicability of the elasticity theory, where  $l$  is a typical molecular dimension. As the additional contribution arises from an entropic origin, we write the additional free energy *density* with the following combinations of the thermal energy and the above two lengths:  $\Delta F = k_B T q_c^2 / \xi + k_B T q_c / \xi^2$ . In the mean field model  $K = K_o S^2$  and  $\Delta\epsilon = \Delta\epsilon_a S$ , and we can write  $\xi(E) = \gamma \sqrt{S} |E|$ , where the constant  $\gamma = \left( \frac{K_o}{\epsilon_o \Delta\epsilon_a} \right)^{\frac{1}{2}}$ . Thus

$$\Delta F = \frac{\mu T}{\sqrt{S}} |E| + \frac{\nu T}{S} E^2 \quad (10)$$

where  $\mu = k_B q_c^2 / \gamma$ , and  $\nu = k_B q_c / \gamma^2$ , are constants and  $\nu \ll \mu$ . We have shown elsewhere [11] that the above form of  $\Delta F$  can be obtained from a simple physical model treating the director fluctuation as a random variable. Calculations based on the total free energy including the director fluctuations show that both  $\delta S(E)$  and  $\Delta T_{PN}(E)$  predominantly vary as  $|E|$  [11].

### 4.3 Order parameter susceptibility: generation of third harmonic component of the electrical signal

We measure the *low frequency* dielectric response of the medium. As we will show below, the nonlinear (field-dependent) dielectric constant generates higher harmonics of the low frequency response. Considering only the capacitive response, the current through the cell is given by  $I = d/dt[C_S V(t)]$  where  $C_S = C_0 \epsilon_{\perp}$ ,  $C_0$  being the capacitance of the empty cell and  $V(t) = V_0 \sin \omega t$  the applied voltage,  $\epsilon_{\perp} = \bar{\epsilon} - \frac{1}{3} \Delta\epsilon_a S(E)$ , and

$$S(E) = S(0) + C_l |E| + C_q E^2 \quad (11)$$

$|E| = |E_o \sin \omega t|$  can be expanded in a Fourier series:

$$|E| = |E_o \sin \omega t| = \frac{2}{\pi} E_o \left[ 1 - \frac{2}{3} \cos 2\omega t - \frac{2}{15} \cos 4\omega t + \dots \right] \quad (12)$$

The capacitive current flowing through the cell can now be calculated. The voltage  $V_m$  measured across the capacitance  $C_m$  (see Fig. 4) is given by  $V_m = I / \omega C_m$ , and the component at the frequency of the applied voltage is given by:

$$V_{1\omega} = \frac{C_0 V_0}{C_m} \left[ \bar{\epsilon} - \frac{\Delta\epsilon_a}{3} S(0) - \frac{8}{9\pi} \Delta\epsilon_a \frac{V_0}{d} C_l - \frac{\Delta\epsilon_a}{4} \frac{V_0^2}{d^2} C_q \right] \quad (13)$$

The quantity in brackets is  $\epsilon_{\perp}$ , which is enhanced with the applied voltage as shown in Figure 5b. The third harmonic signal, which has contributions from both the  $2\Omega$  and  $4\Omega$  components in equation (12), is given by

$$V_{3\omega} = \frac{\Delta\epsilon_a}{d} \frac{C_0}{C_m} \left[ \frac{8}{15\pi} C_l V_o^2 + \frac{C_q}{4d} V_o^3 \right] \quad (14)$$

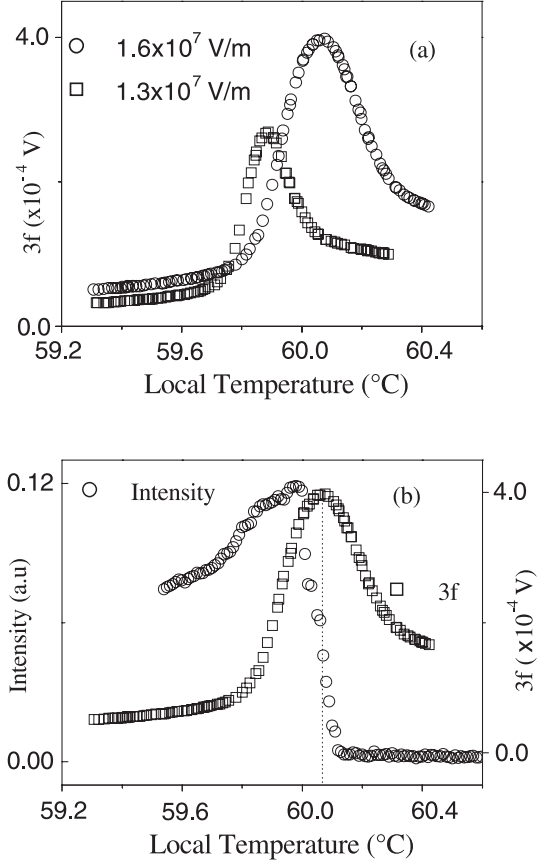


**Fig. 11.** (a) Variations of the third harmonic ( $3f$ ) electrical signals as functions of local temperature. Applied field:  $1.6 \times 10^7$  V/m (circles) and  $1.3 \times 10^7$  V/m (squares), frequency: 1111 Hz. (b) Variations of transmitted intensity as well as the third harmonic electrical signal as functions of local temperature at  $1.6 \times 10^7$  V/m: dotted vertical line denotes the PN transition temperature corresponding to the peak in the  $3f$  signal.

$V_{3\omega}$  depends only on the field enhancement in the order parameter, and hence on the susceptibilities  $C_l$  and  $C_q$ .

We have simultaneously measured the first ( $f$ ), second ( $2f$ ) and third ( $3f$ ) harmonic electrical signals as well as the transmitted intensity as functions of *local temperature* near the paranematic-nematic transition point. The  $3f$  signal shows a clear peak only at relatively high fields, indicating that the transition has become second ordered in nature. Variations of  $3f$  signals at  $1.3 \times 10^7$  V/m and  $1.6 \times 10^7$  V/m at the frequency of 1111 Hz are shown in Figure 11a. This frequency was chosen to get reasonable higher harmonic signals. As we mentioned earlier, there is some misalignment of the director above  $1.1 \times 10^7$  V/m. However, this does not affect the electrical measurements which essentially sense only  $\epsilon_{\perp}$  at high fields. The  $3f$  signal at  $1.3 \times 10^7$  V/m shows a nearly symmetric narrow peak at  $59.89^{\circ}\text{C}$ . Its value at the peak ( $\sim 2.8 \times 10^{-4}$  V) is  $\sim 6$  times larger than that of the background signal. At  $1.6 \times 10^7$  V/m the peak occurs at a higher temperature ( $60.08^{\circ}\text{C}$ ). The signal at the peak ( $\sim 4 \times 10^{-4}$  V) is  $\sim 8$  times larger than the background signal. We have

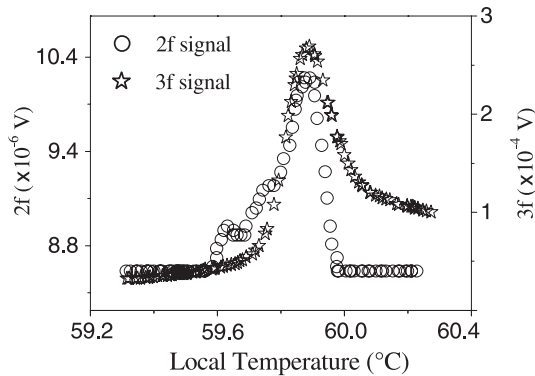


**Fig. 12.** Variations of third ( $3f$ ) and second ( $2f$ ) harmonic electrical signals across the paranematic-nematic transition region as functions of local temperature. Applied field:  $1.3 \times 10^7$  V/m, frequency: 1111 Hz.

estimated the tricritical field to be  $\simeq 1.7 \times 10^7$  V/m for  $\Delta\epsilon_a = -10$ , from the electric field phase diagram given in reference [3]. Optical measurements could not be used to measure the order parameter  $S$  beyond  $1 \times 10^7$  V/m, and hence we could not precisely locate the tricritical point. As we mentioned earlier the steep variation of  $\epsilon_{\perp}$  upto  $9.8 \times 10^6$  V/m indicates that the transition is first ordered whereas the variation of  $\epsilon_{\perp}$  beyond  $1.3 \times 10^7$  V/m is smooth and gradual, indicating that the transition has become second ordered (see Fig. 5b). Further the electrical measurement shows a clear peak in the third harmonic signal and hence we believe that the field induced  $N_{U-}$  to  $N_B$  transition becomes tricritical near  $1.3 \times 10^7$  V/m. The lower experimental value of the tricritical field compared to the calculated one probably arises from the contribution of the field quenching of the director fluctuations to the thermodynamics of the PN transition.

From the data shown in Figure 11 we find that in the nematic phase  $V_{3\omega}$  is  $\propto V_0^2$  rather than  $V_0^3$ . For example at  $59.4$  °C,  $V_{3\omega}/V_0^2$  is  $8.5 \times 10^{-10}$  V $^{-1}$  at  $1.3 \times 10^7$  V/m and  $8.4 \times 10^{10}$  V $^{-1}$  at  $1.61 \times 10^7$  V/m. At  $59.6$  °C this ratio increases to  $1.1 \times 10^{-9}$  V $^{-1}$  and  $1.0 \times 10^{-9}$  V $^{-1}$ . On the other hand, in the paranematic phase,  $V_{3\omega}$  is  $\propto V_0^3$ . For example at  $60.3$  °C,  $V_{3\omega}/V_0^3$  is  $1.4 \times 10^{-11}$  and  $1.3 \times 10^{-11}$  V $^{-2}$  respectively for the same applied fields. Thus it is clear that even at the high fields which are above the tricritical value, the main contribution to the susceptibility arises from the quenching of director fluctuations in the nematic phase. On the other hand, in the paranematic phase, the Kerr effect makes the dominant contribution to the susceptibility.

We show the variations of the  $3f$  signal as well as the transmitted intensity in Figure 11b as functions of the local temperature at  $1.6 \times 10^7$  V/m. The temperature at which the  $3f$  signal shows a peak ( $60.08$  °C) is indicated by a vertical dotted line (see Fig. 11b). It occurs at the middle of the steep variation of the transmitted intensity which is hence the actual bulk PN transition temperature.

Under a strong electric field, the PN transition becomes second ordered and the dipole moments of the molecules may get correlated over large domains near this

transition. Due to the slow dynamics near the transition point the domains may not be able to reorient at the frequency of the applied field. As a result a second harmonic electrical signal ( $2f$ ) can be generated [8]. The variation of measured  $2f$  component of the electrical signal across the paranematic-nematic transition at  $1.3 \times 10^7$  V/m is shown in Figure 12. There is some background signal due to the nonlinearity of the voltage amplifier. However near the PN transition point, a small peak in  $2f$  signal which is  $\sim 20\%$  higher than the background is seen and it occurs at the same temperature as that of the peak in the  $3f$  component (Fig. 12). It probably indicates the presence of polarized domains that do not reorient with the field [8].

## 5 Conclusions

We have presented the high electric field phase diagram of a nematic liquid crystal with  $\Delta\epsilon < 0$ . In the nematic phase the field induced enhancement in the order parameter is analysed using the Kerr effect as well as the quenching of macroscopic director fluctuations by the field. The temperature variations of the relevant susceptibilities ( $C_q$  and  $C_l$ ) indicate that the latter contribution dominates. The uniaxial negative order parameter ( $S_{U-}$ ) in the paranematic phase is estimated from the dielectric constant data. It varies as  $E^2$  indicating that the contribution comes from the Kerr effect only. Our measurements as well as the data available in the literature show that under an electric field the paranematic-nematic transition temperature ( $T_{PN}$ ) varies *linearly* with  $|E|$  in both materials with  $\Delta\epsilon < 0$  and  $\Delta\epsilon > 0$ . It is argued that the quenching of the director fluctuations under strong electric fields significantly contributes to the thermodynamics of the nematic to paranematic transition. At relatively high fields, the third harmonic electrical signal which is a measure of the susceptibility of the medium exhibits a peak at the transition temperature indicating that the transition has become second ordered. Analysis of the third harmonic signal also shows that near  $T_{PN}$  the main contribution to the order parameter susceptibility of the nematic phase comes from the quenching of the director fluctuations even at high fields. The detection of a very small, sharp peak in the second harmonic signal which arises at the same temperature where the third harmonic signal diverges indicates the presence of polarised domains near the transition point.

Our results illustrate the dominant contribution made by the quenching of (transverse) director fluctuations by the external field to various measured properties. A rigorous theoretical model of the electric field phase diagram should take into account this effect, even when the transition is first ordered. Near the critical point in materials with  $\Delta\epsilon > 0$  and above the tricritical point in materials with  $\Delta\epsilon < 0$ , the fluctuations in the magnitude of order parameter also should contribute to the problem.

## References

1. P.G. de Gennes, J. Prost, *The Physics of Liquid Crystals* (Clarendon Press, Oxford, 1993)
2. E.F. Grasmbergen, L. Longa, W.H. de Jeu, *Phys. Rep.* **135**, 195 (1986)
3. C. Fan, M.J. Stephen, *Phys. Rev. Lett.* **25**, 500 (1970)
4. A.J. Nicastro, P.H. Keyes, *Phys. Rev. A* **30**, 3156 (1981)
5. L. Lelidis, G. Durand, *Phys. Rev. E* **48**, 3822 (1993)
6. L. Lelidis, M. Nobili, G. Durand, *Phys. Rev. E* **48**, 3818 (1993)
7. G. Basappa, N.V. Madhusudana, *Mol. Cryst. Liq. Cryst.* **288**, 161 (1996)
8. G. Basappa, N.V. Madhusudana, *J. Eur. Phys. B* **1**, 179 (1998)
9. B. Malraison, Y. Poggi, E. Guyon, *Phys. Rev. A* **21**, 1012 (1980)
10. D.A. Dunmur, K. Szumilin, T.F. Waterworth, *Mol. Cryst. Liq. Cryst.* **149**, 385 (1986); D.A. Dunmur, K. Szumilin, *Liq. Cryst.* **6**, 449 (1989); P.P. Muhoray, D.A. Dunmur, *Mol. Cryst. Liq. Cryst.* **97**, 337 (1983); D.A. Dunmur, P.P. Muhoray, *J. Phys. Chem.* **92**, 1406 (1988)
11. S. Dhara, N.V. Madhusudana, *Europhys. Lett.* **67**, 411 (2004)
12. M. Sorai, in *Liquid Crystals: Nematics*, edited by D. Dunmur, A. Fukuda, G.R. Luckhurst (INSPEC, London, 2000), p. 141
13. I. Haller, H.A. Huggins, H.R. Lilienthal, T.R. McGuire, *J. Phys. Chem* **77**, 950 (1973)
14. P. Sheng, *Phys. Rev. A* **26**, 1610 (1982)
15. W. Helfrich, *Z. Naturforsch.* **33a**, 305 (1978)
16. S. Dhara, N.V. Madhusudana, *Eur. Phys. J. E* **13**, 401 (2004)

Copyright of European Physical Journal E -- Soft Matter is the property of Springer Science & Business Media B.V. and its content may not be copied or emailed to multiple sites or posted to a listserv without the copyright holder's express written permission. However, users may print, download, or email articles for individual use.